A Simple Optimization Method for Generating High-Purity Amplitude and Phase Modulation

Archita Hati, *Member, IEEE*, and Craig W. Nelson, *Member, IEEE*

***Abstract*— We present a simple method for the adjustment of an in-phase (I) and quadrature-phase (Q) Armstrong-type modulator for use as a calibrator in precision noise metrology. The availability of relatively pure levels of both amplitude modulation (AM) and phase modulation (PM) can greatly simplify the optimal alignment and calibration of metrology equipment, such as AM and PM noise measurement systems. The phase and amplitude imbalance of the components that constitute an IQ modulator results in an undesired combination of AM and PM. These impairments must be corrected to generate the pure signals required for metrology. Our proposed method corrects for these nonideal impairments without needing a calibrated IQ demodulator and offers a high-purity AM/PM signal with spurious modulations as low as 1 ppm. We present the calibration procedure and uncertainty analysis of such a modulator when used as a calibrator for a PM and AM noise measurement system.**

***Index Terms*— Amplitude modulation (AM), Armstrong modulator, in-phase and quadrature-phase (IQ) modulator, phase modulation (PM), phase noise, single sideband (SSB) modulation, uncertainty.**

I. Introduction

FOR precision amplitude modulation (AM) and phase modulation (PM) noise measurements [1]–[5], an accurate determination of measurement system sensitivity is important. Historically, Armstrong [6]–[8], single sideband (SSB), and additive noise modulators have been utilized for this purpose [9]–[13]. Adjustment and preservation of orthogonality between a measurement system's AM and PM sensitivity are also of utmost importance. Ideally, for PM noise, the measurement system needs to be insensitive to AM fluctuations, and the converse is true for AM measurements. The flexible and adjustable Armstrong modulator can be invaluable for tuning the AM–PM balance in some measurement systems. This type of modulator generates double-sideband suppressed-carrier (DSB-SC) AM by frequency mixing a baseband signal with a coupled portion of the carrier. The original carrier is then combined with the phase-shifted DSB-SC signal. The amount of phase shift introduced controls the balance between the generated AM and PM of the carrier.

A modern implementation of the Armstrong modulator replaces the frequency mixing element with an in-phase and quadrature-phase (IQ) mixer driven by a dual direct digital synthesizer (DDS).

Manuscript received 9 March 2022; revised 8 June 2022; accepted 13 June 2022. Date of publication 27 June 2022; date of current version 20 July 2022. The Associate Editor coordinating the review process was Dr. Helko E. Van Den Brom. *(Corresponding author: Archita Hati.)*

The authors are with the National Institute of Standards and Technology, Boulder, CO 80305 USA (e-mail: archita.hati@nist.gov; nelson@nist.gov).

Digital Object Identifier 10.1109/TIM.2022.3186367

The IQ-based modulator can easily be reconfigured *in situ* to generate AM, PM, or SSB modulation by simply adjusting the DDS signals. Imperfections such as gain and phase imbalance in the IQ modulator can also be easily compensated for by adjusting the DDS parameters. Our proposed method corrects for these nonideal impairments and offers operation of the modulator with spurious modulations as low as 1 ppm without the need for any additional hardware, unlike as described in [12], where an IQ demodulator is used for the adjustment of the modulator imperfections. In the proposed method, the compensation of the IQ impairments is realized by the optimization of a generated SSB signal. It relies on the fact that perfect SSB generation is only achieved when the modulator imbalances are compensated for.

In this article, we describe the operation and optimization method for the IQ-based AM/PM modulator and provide an experimental demonstration. We present the calibration procedure, sources of measurement errors, measurement equation, and uncertainty analysis of such a modulator.

II. Brief Overview of AM, PM, and SSB Modulation

The basic model for a signal, $\mathrm{v}_{RF}(t)$, with amplitude and phase fluctuations, can be represented as

$$\mathrm{v}_{RF}(t) = A(1+\alpha(t))\cos(\omega_c t+\varphi(t)) \tag{1}$$

where A, $\alpha(t)$, ω_c, and $\varphi(t)$ are the amplitude, fractional amplitude fluctuations, average carrier frequency, and phase fluctuations, respectively. In noise metrology, AM noise, represented as $S_\alpha(f)$, is the one-sided double-sideband power spectral density of fractional amplitude fluctuations. Similarly, PM noise, represented as $S_\varphi(f)$, is the one-sided double-sideband power spectral density of phase fluctuations [14]. $S_\alpha(f)$ and $S_\varphi(f)$ are expressed in units of 1/Hz and rad^2/Hz, respectively, and f is the Fourier (or offset) frequency from the carrier that ranges from 0 to ∞.

In this document, since we will be discussing single-tone sinusoidal modulation, the notation S_α (unitless) and S_φ (rad^2) will be used to represent the power spectrum of AM and PM instead of power spectral density.

For sinusoidal AM, we set

$$\alpha(t) = m_\alpha\cos(\omega_m t) \quad \text{and} \quad \varphi(t)=0 \tag{2}$$

where $\omega_m = 2\pi f_m$, f_m, and m_α are the modulation frequency and AM depth, respectively. Sinusoidal AM produces radio frequency (RF) and AM power spectra, as shown in Fig. 1(a).

For sinusoidal PM, we set

$$\alpha(t) = 0 \text{ and } \varphi(t) = m_\varphi\cos(\omega_m t) \tag{3}$$

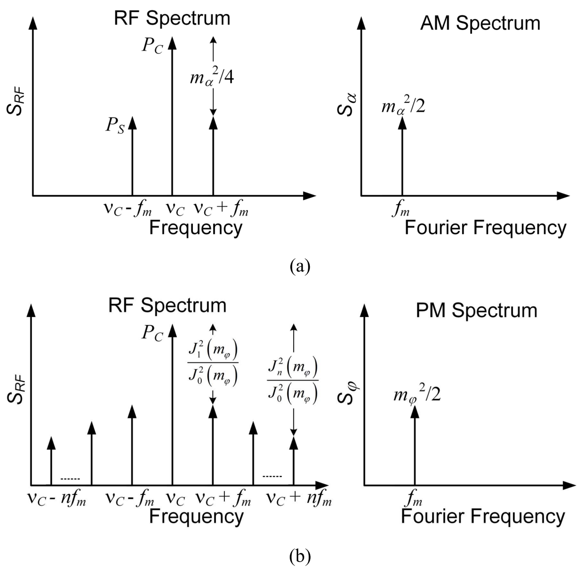

Fig. 1. RF spectrum, AM, and PM spectrum of single-tone sinusoidal modulation. (a) AM. (b) PM. For the PM case, the harmonic distribution of the RF spectra can be described with the Bessel functions (J_n). Odd harmonics have a phase inversion between the USB and LSB. P_C and P_S are the carrier and sideband power, respectively.

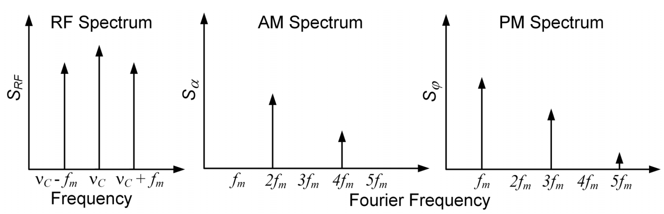

Fig. 2. Truncated RF spectrum of a phase-modulated signal generated with a single pair of sidebands. The AM and PM spectra contain the even and odd harmonics of the modulating frequency, respectively.

where m_φ is the PM depth. The RF spectrum of the phase-modulated signal consists of a harmonic distribution of sidebands, as shown in Fig. 1(b), and can be described with the Bessel functions of the first kind, $J_n(m_\varphi)$ (n is a positive integer). For PM, odd harmonics of the modulating frequency have a phase inversion between the upper sideband (USB) and lower sideband (LSB). Also, for small modulation depths, most of the modulation power exists in the first pair of sidebands.

An approximated sinusoidal phase modulated signal can be generated with only a single pair of RF sidebands instead of the complex RF spectra described by the Bessel functions. This is the type of PM generated with an Armstrong modulator [1]. The missing higher order RF sidebands necessary for pure PM result in spurious AM at even harmonics and PM at odd harmonics of the modulation frequency (see Fig. 2). For small modulation depths ($m_\varphi \ll 0.1$), the approximation of pure PM can be quite good.

Finally, an SSB modulated signal can be generated by combining a pair of in-phase (I) sidebands with a set of out-of-phase sidebands and expressed as [15]

$$\mathrm{v}_{RF}(t) = m(t)\cos(\omega_c t) \mp m_H(t)\sin(\omega_c t) \tag{4}$$

where $m(t)$ is the modulating signal and $m_H(t)$ is the Hilbert transform of $m(t)$. The $-$ and $+$ sign of $m_H(t)$ produce the

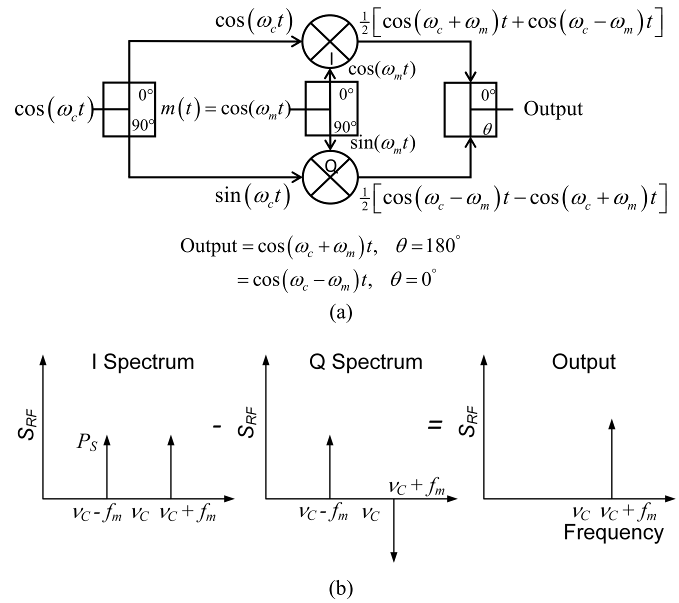

Fig. 3. (a) IQ mixer-based SSB modulator. (b) RF spectra for the I path, Q path, and output of the modulator for $\theta = 180°$. A perfect SSB signal is generated when the I and Q path signals are in perfect quadrature and have equal amplitude responses.

USB and LSB, respectively. This is typically done with an IQ modulator driven with a 90° hybrid at the I and Q modulation ports, as shown in Fig. 3.

The modulator described in this article is the modern implementation of the Armstrong modulator, and it uses SSB modulation as an indicator for the generation of near-perfect AM and PM.

III. IQ-Based Armstrong Modulator for AM and PM Generation

The block diagram of the proposed modulator is shown in Fig. 4. A small portion of the carrier signal is coupled out at the input port, mixed with the baseband signals using an IQ mixer resulting in suppressed-carrier modulation, which is finally coupled back into the direct signal path at the output port. By adjusting the phase and amplitude relationship of the two baseband modulating signals, any combination of AM and PM or even SSB modulation can be generated. However, an IQ modulator deviates from its ideal model due to several impairments, such as IQ amplitude imbalance (ε) and phase imbalance (ψ), which breaks the orthogonality of the system, insertion phase shift (θ) of the modulated signal, and mismatch of the mixer diodes, which results in a dc offset and imperfect carrier suppression.

The nonideal modulator can be modeled as an ideal modulator with all impairments realized as a 2 × 2 matrix (M_{impair}) multiplication at the I and Q baseband inputs. The inversion of M_{impair} results in a correction matrix that can be applied at the I and Q inputs to compensate for these impairments. We model the amplitude and phase imbalances at the 90° hybrid that is connected to the local oscillator (LO) port of the mixers, and the corresponding impairment matrix is given by

$$M_{impair} = \frac{1}{2}\begin{bmatrix} \cos(\theta) & -(1+\varepsilon)\sin(\theta+\psi) \\ \sin(\theta) & (1+\varepsilon)\cos(\theta+\psi) \end{bmatrix}. \tag{5}$$

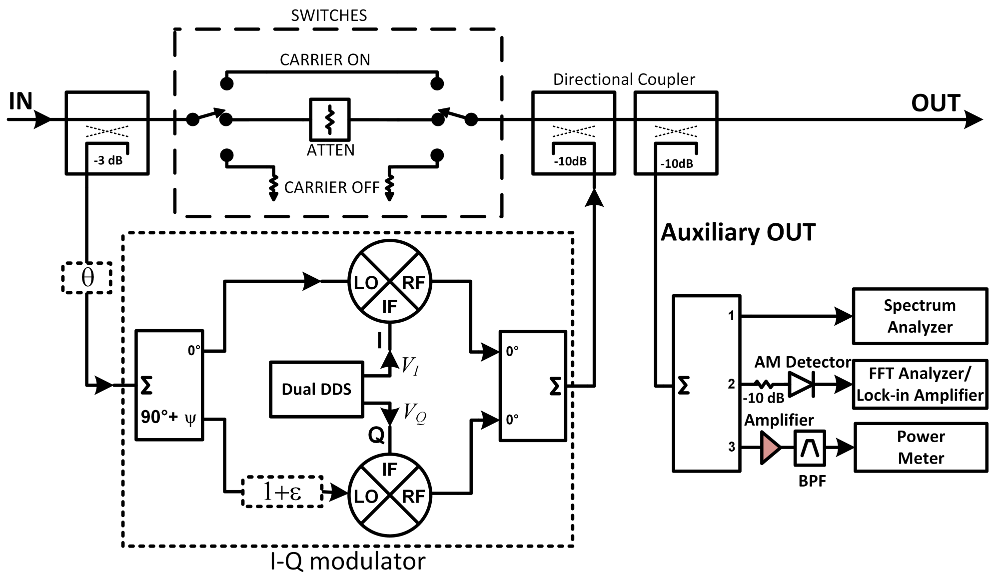

Fig. 4. Block diagram of the proposed modulator for generating high-purity AM and PM signals. Here, the AM and PM modulated signals are created by adding a DSB-SC signal to the original carrier. High-purity AM and PM are achieved by optimizing the IQ mixer parameters and looking for high-quality SSB generation. θ, ε, and ψ describe the nonideal impairments of the modulator. The amplifier for the power measurement is optional.

TABLE I
DDS PHASE AND AMPLITUDE SETTINGS FOR SSB

SSB Selection	I DDS		Q DDS	
	Amplitude (Volt)	Phase (radian)	Amplitude (Volt)	Phase (radian)
Lower Sideband (LSB)	V_m	ψ	$\frac{V_m}{(1+\varepsilon)}$	$\frac{\pi}{2}$
Upper Sideband (USB)	V_m	$\frac{\pi}{2}$	$\frac{V_m}{(1+\varepsilon)}$	ψ

V_m, ψ, ε are the baseband modulation amplitude, phase imbalance, and amplitude imbalance, respectively.

Multiplying the I and Q signals with the inverse impairment matrix (M_{impair}^{-1}) corrects for the impairments in the modulator. The corrected I and Q signals are represented by

$$\begin{bmatrix} V_I(t) \\ V_Q(t) \end{bmatrix} = M_{impair}^{-1} \begin{bmatrix} V_I'(t) \\ V_Q'(t) \end{bmatrix} \tag{6}$$

where

$$M_{impair}^{-1} = 2\sec(\psi) \begin{bmatrix} \cos(\theta+\psi) & \sin(\theta+\psi) \\ -\frac{\sin(\theta)}{(1+\varepsilon)} & \frac{\cos(\theta)}{(1+\varepsilon)} \end{bmatrix} \tag{7}$$

where $V_I(t)$, $V_Q(t)$, $V_I'(t)$, and $V_Q'(t)$ represent the corrected and uncorrected I and Q signals, respectively. Also, for simplicity, dc offset impairments are not included in (5).

A dual DDS is connected to the I and Q ports of the modulator. Having the DDS under computer control allows for fine adjustments of differential phase, amplitude, and dc offsets between both signals. By implementing (6) and (7) in software, the impairment corrected I and Q signals can be generated by the DDS.

The necessary steps needed to optimize the modulator are listed below.

A. Initialize the Dual DDS

Set the phase and amplitude for both the I and Q DDSs as described in Table I. Start with the LSB and set $\psi = \varepsilon = 0$. Also, set the frequency of both DDS equal to f_m.

B. Optimize Carrier Suppression

1) Turn off the carrier readdition switch (switch in the CARRIER OFF position).

2) Adjust dc offsets of I and Q DDSs iteratively to maximize carrier suppression at the output.

C. Adjust Parameters to Generate Pure SSB

Since SSB can be created by the superposition of pure AM and pure PM, we can use this concept to create an "ideal" IQ-modulator by correcting the amplitude and phase imbalances.

1) Adjust phase (ψ) and amplitude (ε) imbalances by adjusting the DDS settings as defined in Table I to minimize unwanted sideband at the output. Adjusting phase, then amplitude in ever-decreasing iterative steps until the undesired level of the sideband no longer decreases or becomes undetectable.
2) Record the values of ψ and ε.
3) Change to the USB setting to verify that the sideband rejection is similar to the LSB setting with the same ψ and ε.

D. Adjust Parameters for Pure PM

1) Turn on the carrier readdition switch (switch in the CARRIER ON position).

2) Set the phase and amplitude for both the I and Q DDSs as described in Table II. Start with PM, $\theta = 0$, and use ψ and ε as determined from step C2).

3) Monitor AM on a detector at the auxiliary output (see Fig. 4). Use a lock-in detector, if available.

4) Adjust insertion phase (θ) until detected AM at f_m is nulled. Also, record the power ratio (κ) of the minimum to maximum detected AM power as θ is varied.

E. Toggle Between AM and PM

Adding or subtracting 90° to θ as determined from step D4) will toggle between AM and PM generation.

TABLE II

DDS PHASE AND AMPLITUDE SETTINGS FOR AM AND PM GENERATION

AM/PM Selection	I DDS Amplitude (Volt)	I DDS Phase (radian)	Q DDS Amplitude (Volt)	Q DDS Phase (radian)
AM	$2\sec(\psi)V_m\cos(\theta+\psi)$	0	$-2\sec(\psi)\frac{V_m}{(1+\varepsilon)}\sin(\theta)$	0
PM	$2\sec(\psi)V_m\sin(\theta+\psi)$	0	$2\sec(\psi)\frac{V_m}{(1+\varepsilon)}\cos(\theta)$	0

V_m, ψ, ε, θ are the baseband modulation amplitude, phase imbalance, amplitude imbalance, and insertion phase shift, respectively. Negative DDS amplitudes can be converted to positive quantities by adding π to the phase.

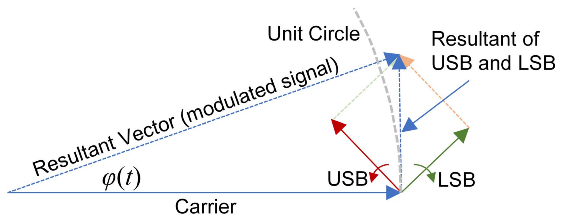

Fig. 5. Vector diagram of the Armstrong modulation. USB is the upper sideband, and LSB is the lower sideband. Since the proposed modulator adds only a single pair of dominant sidebands to the carrier, the resultant vector representing the phase-modulated carrier deviates from the unit circle and produces spurious AM at the even harmonics of modulating frequency, as shown in Fig. 2.

The same procedure can be repeated at different f_m values to determine the frequency response of the modulator.

IV. CALIBRATION PROCEDURE AND ESTIMATION OF UNCERTAINTY

The accurate determination of the modulation depth of the AM/PM modulator used as a calibrator in precision noise metrology is of utmost importance. In this section, we describe the calibration procedure and define the measurement equation for the PM and AM modulator. The calibration procedure relies on the fact that the modulation depth (m_α and m_φ) can be determined from the ratio between the power in the first pair of sidebands ($P_{DSB} = 2P_S$) and the carrier power (P_C).

For the AM case, the modulation depth, m_α, describes the fractional peak AM. It can be calculated from the sideband-to-carrier power ratio [12], [16]

$$m_\alpha = \sqrt{\frac{2P_{DSB}}{P_C}}. \tag{8}$$

The proposed modulator adds only a single pair of dominant sidebands to the carrier. If the amplitudes of the modulation signals (I and Q) are much smaller than the amplitude of the LO signal on the mixer, one can ignore the high-order modulation sidebands. Moreover, the modulating sidebands are readded to the carrier with a directional coupler, and this path has an unknown insertion phase (θ). For the PM case, the sidebands are rotated to compensate for this insertion phase shift, so that they produce a 90° relationship with respect to the carrier, as indicated in Fig. 5. The resultant of the USB and LSB is tangential to the unit circle for a single pair of sidebands. In contrast, for the AM case, the sidebands are rotated, so that the resultant of the USB and LSB is in line with the carrier.

Since m_φ is also an indicator of peak phase deviation, from simple geometry, it can be determined as the arctangent of the

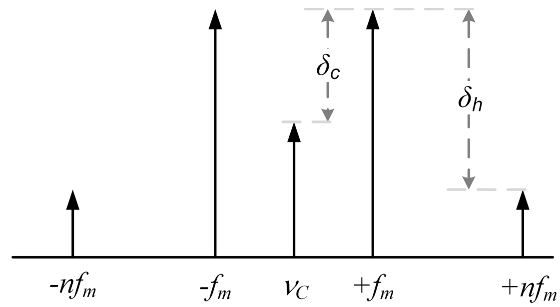

Fig. 6. Spectrum representing the unsuppressed carrier and higher order harmonic terms due to the nonideal behavior of the modulator.

first pair of sidebands-to-carrier power ratio as

$$\begin{aligned} m_\varphi &\cong \tan^{-1}\left(\sqrt{\frac{2P_{DSB}}{P_C}}\right), \quad \text{for } m_\varphi < \frac{\pi}{4} \\ &\cong \sqrt{\frac{2P_{DSB}}{P_C}}, \quad \text{for } m_\varphi < 0.1. \end{aligned} \tag{9}$$

The small-angle approximation for the arctangent is often used for small modulation levels.

A. Calibration Procedure

The measurement setup for calibration of the modulator is shown in Fig. 4. Accurate measurement of signals with vastly different power levels ($P_C >> P_{DSB}$) can be difficult because it requires a high level of linearity in the power meter. This problem can be circumvented by using a calibrated attenuator to ensure that the power meter operates at nearly the same power level for both measurements (Fig. 4). However, to automate the process of incorporating the AM/PM modulator into a measurement system, we need to include switches, directional couplers, AM detector, bandpass filter (BPF), and an amplifier. The amplifier is optional, it may be required to increase the signal-to-noise ratio (SNR) for the power measurements. The BPF filter is used to prevent bias from the higher-order harmonics of the carrier during the power measurement.

The procedure for calibration is as follows:

1) **Measure Carrier Power**
   1) Set the switch position to "ATTN."
   2) Turn off modulation signals from the dual DDS.
   3) Measure attenuated carrier power $P_C{}'$.
2) **Measure Sideband Power**
   1) Set switch position to "CARRIER OFF."
   2) Configure the DDSs for PM (or AM).
   3) Measure modulation sideband power P_{DSB}.
   4) Observe the signal on a spectrum analyzer and record the power ratio, δ_c, between the unsuppressed carrier at ν_c and the modulation sideband at f_m (see Fig. 6).
   5) Record power ratio, δ_h, of the largest harmonic of modulation frequency, at nf_m, relative to the main sideband at f_m (see Fig. 6).

B. Measurement Equation for the PM Modulator

We are only interested in the modulation depth of the first spectral component of the modulation as we will use it as the calibration tone for AM and PM noise metrology. Therefore, we require an accurate measurement of the power ratio between the carrier and the first pair of sidebands. The guide to the expression of uncertainty in measurement (GUM) [17] states, "the uncertainty of a measurement should be calculated by propagating the uncertainty of contributing factors relevant to the measurement" and is "usually evaluated using a mathematical model of the measurement." We have constructed an equation that models (9) and accounts for possible measurement errors and biases. The proposed measurement equation for the PM depth, m_φ, can be written as

$$m_\varphi = \tan^{-1}\left(\sqrt{\frac{2}{K_{SW}K_{PNL}K_{\delta c}K_{\delta h}}\frac{P_{DSB}\left(1-\frac{1}{SNR}\right)}{AP_C'\left(1-\frac{1}{SNR'}\right)}}\right) \quad (10)$$

where $P_C{}'$ is the attenuated carrier power, P_{DSB} is the sideband power, and A is the attenuation factor ($A \geq 1$). SNR and SNR′ are the signal-to-noise ratio for the total sideband power measurement and attenuated carrier power measurement, respectively. K_{SW} is a term for propagating uncertainty for the different switched paths. This quantity includes the repeatability of the switches, insertion loss, and voltage standing wave ratio (VSWR) differences. K_{PNL} accounts for power meter nonlinearity between the attenuated carrier and sideband power measurements. It also accounts for the nonlinearity of the optional amplifier preceding the power meter. $K_{\delta c}$ is for the compensation of unsuppressed carrier power, and $K_{\delta h}$ accounts for higher order harmonic content of the modulated signal inside the filter bandwidth.

Harmonic distortion from the mixing process can cause biases in the power measurement of the first two sidebands and must be prevented or accounted for. When using a power meter to measure P_{DSB}, the carrier is switched off, and any residual carrier due to the nonideal mixing process or switch leakage creates a measurement bias that can be compensated for. To account for nonlinearity and any unsuppressed carrier, we define $K_{\delta c}$ and $K_{\delta h}$ as follows:

$$\begin{aligned} K_{\delta c} &= 1 + \frac{\delta_c}{2}, \\ K_{\delta h} &= 1 + \delta_h. \end{aligned} \quad (11)$$

Substituting (11) into (10) gives

$$m_\varphi = \tan^{-1}\left(\sqrt{\frac{2}{K_{SW}K_{PNL}\left(1+\frac{\delta_c}{2}\right)(1+\delta_h)}\frac{P_{DSB}\left(1-\frac{1}{SNR}\right)}{AP_C'\left(1-\frac{1}{SNR'}\right)}}\right). \quad (12)$$

For a phase modulated signal with a single pair of sidebands, the PM spectrum at the modulating frequency f_m can be expressed in terms of the Bessel function of m_φ as [16], [18]

$$S_\varphi(f_m) = \frac{2(1-\kappa)J_1^2(m_\varphi)}{J_0^2(m_\varphi)}. \quad (13)$$

The higher order sidebands (nf_m) produce spurious AM at even harmonics of the modulating frequency and spurious PM at odd harmonics, as shown in Fig. 2. In (13), κ is an indicator of the modulator's PM purity and defined as the power ratio of the spurious AM sideband to total sideband power. When the modulator is not creating pure PM, a portion of the sideband power appears as spurious AM and thus reduces the amount of generated PM. This spurious AM can be a result of many imperfections that are not compensated for in the modulator; a few examples are digital-to-analog converter (DAC) quantization and mixer or DAC nonlinearity. All of these uncompensated imperfections do not need to be individually evaluated and tracked; we simply absorb their total effect as uncertainty on κ. The value of κ can be estimated by measuring the ratio between the minimum and maximum detected AM as θ is varied [see Section III, step D4)]. For an ideal modulator, $\kappa = 0$.

Using (13), modulation depths as large as $m_\varphi = 1$ can be used with an error of less the 0.1 dB in $S_\varphi(f)$. For low levels of modulation ($m_\varphi \ll 0.1$), one or more of the terms of the Taylor expansion can be used for simplicity. Therefore

$$S_\varphi(f_m) = (1-\kappa)\left(\frac{m_\varphi^2}{2} + \frac{m_\varphi^4}{8} + \frac{11m_\varphi^6}{384} + O\left(m_\varphi^7\right)\right). \quad (14)$$

C. Measurement Equation for the AM Modulator

The equation that describes the power ratio measurement for the determination of m_α can be written as

$$m_\alpha = \sqrt{\frac{2}{K_{SW}K_{PNL}\left(1+\frac{\delta_c}{2}\right)(1+\delta_h)}\frac{P_{DSB}\left(1-\frac{1}{SNR}\right)}{AP_C'\left(1-\frac{1}{SNR'}\right)}}. \quad (15)$$

The AM spectrum can be expressed in terms of m_α as

$$S_\alpha(f_m) = (1-\gamma)\frac{m_\alpha^2}{2}. \quad (16)$$

The term γ is an indicator of the modulator's AM purity and is defined as the power ratio of the spurious PM sideband to total sideband power. For an impairment-corrected modulator $\gamma = \kappa$, and since κ is much easier to determine, this is a useful identity.

We define a figure of merit (FOM) for the purity of the modulator as κ and γ for the PM and AM, respectively.

Substitution of (15) in (16) yields

$$S_\alpha(f_m) = \frac{(1-\gamma)}{K_{SW}K_{PNL}\left(1+\frac{\delta_c}{2}\right)(1+\delta_h)}\frac{P_{DSB}\left(1-\frac{1}{SNR}\right)}{AP_C'\left(1-\frac{1}{SNR'}\right)}. \quad (17)$$

The equation for AM depth (15) is similar to (12), however, without the arctangent since the AM Cartesian resultant is in-line with the carrier as opposed to in quadrature. Likewise, the measurement equation for AM created by the modulator is given in (17) and can be used for large modulation indexes. When using an impairment-corrected modulator at small modulation depths, m_α and m_φ are nearly equal. Therefore, the calibration for the PM case can be reused. A simplified expression for S_α in terms of S_φ is given in (18). Since we calibrated the modulator for pure PM by using an AM null measurement, any residual uncorrected amplitude imbalance appears directly as an imbalance between the AM and PM levels. A correction factor κ_{ssb} is introduced, such that

$$S_\alpha(f_m) \approx \kappa_{ssb}S_\varphi(f_m) \quad \text{when} \quad m_\varphi(f) \ll 0.1. \quad (18)$$

We define $\kappa_{ssb} = (1 \pm \varepsilon_{ssb})$, where ε_{ssb} represents the effective residual amplitude imbalance after impairment correction. It can be determined while creating SSB by measuring the power ratio δ_{ssb} of the suppressed sideband to the desired unsuppressed sideband on a spectrum analyzer and can be expressed as

$$\varepsilon_{ssb} = \left(\frac{1+\sqrt{\delta_{ssb}}}{1-\sqrt{\delta_{ssb}}}\right)^2 - 1 \quad = \quad \frac{4\sqrt{\delta_{ssb}}}{\left(\sqrt{\delta_{ssb}}-1\right)^2}. \tag{19}$$

The error term is typically small, and determining its correct sign is tedious. For simplicity, we make κ_{ssb} equal to unity with a uniformly distributed uncertainty of $\pm\varepsilon_{ssb}$ for the worse case residual imbalance.

D. Combined Uncertainty

Following the GUM [17], [19], the equation for the combined uncorrelated uncertainties (u_C) for a measurand y is written as

$$\begin{aligned} y &= F(x_1, x_2, \ldots, x_N) \\ u_C^2(y) &= \sum_{i=1}^{N} \underbrace{\left(\frac{\partial F}{\partial x_i}\right)^2}_{\substack{Sensitivity\\ Coefficients}} u^2(x_i) \end{aligned} \tag{20}$$

where F represents the measurement function. In terms of fractional uncertainties, (20) is given by

$$\overbrace{\frac{u_C^2(y)}{y^2}}^{\substack{\text{Total}\\ \text{Fractional}\\ \text{Uncertainty}}} = \sum_{i=1}^{N} \overbrace{\left(\frac{\partial F}{\partial x_i}\right)^2 \frac{x_i^2}{y^2}}^{\text{Multiplier}} \overbrace{\frac{u^2(x_i)}{x_i^2}}^{\substack{\text{ith Component}\\ \text{Fractional}\\ \text{Uncertainty}}}$$

$$\sigma_C^2 = \sum_{i=1}^{N} \overbrace{\left(\frac{\partial F}{\partial x_i}\right)^2 \frac{x_i^2}{y^2}}^{\text{Multiplier}} \overbrace{\sigma_i^2}^{\substack{\text{ith Component}\\ \text{Fractional}\\ \text{Uncertainty}}} . \tag{21}$$

σ^2 is used here to represent the fractional variance. For PM, the multipliers are determined by partial derivative sensitivity analysis of (14). By substituting y equal to S_φ in (21), the individual multipliers are given by

$$\begin{aligned} &\left(\frac{\partial F}{\partial P_{DSB}}\right)^2 \frac{P_{DSB}^2}{S_\varphi^2} = \left(\frac{\partial F}{\partial P_C'}\right)^2 \frac{P_C'^2}{S_\varphi^2} = \left(\frac{\partial F}{\partial A}\right)^2 \frac{A^2}{S_\varphi^2} = 1 \\ &\left(\frac{\partial F}{\partial K_{SW}}\right)^2 \frac{K_{SW}^2}{S_\varphi^2} = \left(\frac{\partial F}{\partial K_{PNL}}\right)^2 \frac{K_{PNL}^2}{S_\varphi^2} = 1 \\ &\left(\frac{\partial F}{\partial \kappa}\right)^2 \frac{\kappa^2}{S_\varphi^2} = \kappa^2 \\ &\left(\frac{\partial F}{\partial SNR}\right)^2 \frac{SNR^2}{S_\varphi^2} = \frac{1}{SNR^2} \\ &\left(\frac{\partial F}{\partial SNR'}\right)^2 \frac{SNR'^2}{S_\varphi^2} = \frac{1}{SNR'^2} \\ &\left(\frac{\partial F}{\partial \delta_c}\right)^2 \frac{\delta_c^2}{S_\varphi^2} = \frac{\delta_c^2}{4} \\ &\left(\frac{\partial F}{\partial \delta_h}\right)^2 \frac{\delta_h^2}{S_\varphi^2} = \delta_h^2. \end{aligned} \tag{22}$$

TABLE III
UNCERTAINTY RULES FOR LOGARITHMIC AND LINEAR QUANTITIES

Operation	**Function, g**	**Fractional Standard Deviation**
Conversion from decibels	$g = 10^{x/a}$ (a = 10 or 20)	$\sigma_g \approx \left\lvert\frac{\ln(10)}{a}\right\rvert \sigma_x$
Conversion to decibels	$g = a\log_{10}(x)$ (a = 10 or 20)	$\sigma_g \approx \left\lvert\frac{a}{\ln(10)}\right\rvert \sigma_x$

The combined fractional variance, σ_{C,S_φ}^2, obtained by combining the individual fractional uncertainties, whether arising from Type A evaluation or Type B evaluation, is

$$\sigma_{C,S_\varphi}^2 = \sigma_{P_{DSB}}^2 + \sigma_{P_C'}^2 + \sigma_A^2 + \sigma_{K_{SW}}^2 + \sigma_{K_{PNL}}^2 + \kappa^2\sigma_\kappa^2 + \delta_h^2\sigma_{\delta_h}^2 + \frac{\delta_c^2\sigma_{\delta_c}^2}{4} + \frac{\sigma_{SNR}^2}{SNR^2} + \frac{\sigma_{SNR'}^2}{SNR'^2}. \tag{23}$$

For the AM case

$$\sigma_{C,S_\alpha}^2 = \sigma_{C,S_\varphi}^2 + \sigma_{\kappa_{ssb}}^2. \tag{24}$$

The expanded uncertainty (U) is equal to $k\sigma_C$, where k is the coverage factor chosen to be 2 for a 95.5 % level of confidence.

Most often, the measurement error of different parameters is available in either logarithmic (decibel, dB) or linear (%) units. For simplicity and consistency, all conversions between logarithmic and linear follow the propagation of uncertainty rules as given in Table III.

V. EXPERIMENTAL RESULTS

After the proposed modulator optimization method was numerically verified with the Labview modulation toolkit, we built and tested two AM and PM modulators operating at 9 MHz and 10 GHz. These two carrier frequencies were generated with a commercial frequency synthesizer (Keysight, E8257D). We used two different IQ mixers (Mini-Circuits ZFMIQ-10M and Marki, MMIQ-0520LSM) but the same dual DDS (Rigol, DG4162) for the 9 MHz and 10 GHz modulators. The dual DDS is a 160 MHz with 14-bit amplitude resolution, 48-bit phase accumulator, and phase noise of approximately −138 dBc/Hz at 10 kHz offset from a 10-MHz carrier. At the auxiliary outputs, a 10-bit fast Fourier transform (FFT) analyzer (Agilent, 89410A) was used to display the power spectrum of the carrier, modulation sidebands, and also the output of a Schottky diode AM detector (Herotek, DHM124AA). The primary output of the modulator was connected to a second FFT analyzer (Agilent, 89410A) that simultaneously displayed the demodulated AM and PM of the carrier (see Fig. 7). The accuracy of the analyzer's demodulating function was verified with an AM/PM secondary noise standard [10], [16] to be within ±0.1 dB. The power measurements at the auxiliary output were performed with a calibrated power meter (HP E4419B/E9300A). All instruments were referenced to

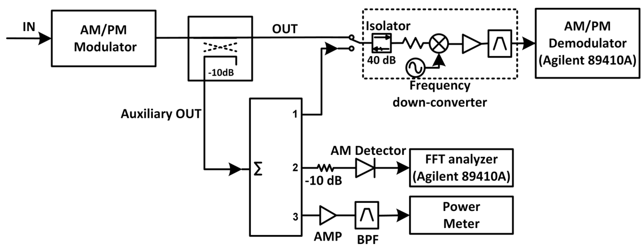

Fig. 7. Block diagram of the experimental setup used for the evaluation of the proposed modulator. The frequency downconverter and the amplifier were only used for the 10-GHz modulator.

the same state-of-the-art 10-MHz quartz oscillator. For the 10-GHz modulator, a downconverter was used to frequency translate the carrier to 9 MHz for analysis on the FFT analyzer. The AM detector and power meter inputs were not routed through the downconverter, as shown in Fig. 7.

Schottky diode detectors, when operating at low input power (<-10 dBm), use the quadratic nature of the diode response to convert power fluctuations to voltage. They are virtually insensitive to phase fluctuations, and this makes them an ideal detector for aligning the modulator for minimum spurious AM [12], [20]. Previous experiments utilizing feedback control loops and diode detectors have created modulators that maintain spurious modulation of less than 1 ppm [13]. When constructing our proposed modulator, it was important to use only linear components such as couplers and splitters between the primary path and the diode detector on the auxiliary path, as this could prevent the minimization of spurious AM at the primary output. To verify that no significant additional spurious AM was generated between the primary output and auxiliary detector, we measured that spurious detection at both outputs was nearly identical (<1 ppm) using the diode detector for the 9-MHz and 10-GHz modulators. We also verified that power measurements between the primary and auxiliary outputs agreed to less than the power meter nonlinearity (<0.05 dB) for the ranges of power needed for carrier and sideband measurements. This was also the case when an amplifier and BPF were inserted before the power meter for the 10 GHz measurements.

First, the dual DDS was configured to generate a 100-kHz upper SSB at a level approximately equal to -35.1 dBc for a 9-MHz carrier. The modulator was optimized with 100 millidegree steps of phase imbalance, 100 milli-dB of amplitude imbalance, and 100 μV of dc offset, the finest resolution that could be used on the dual DDS. The dc offsets were adjusted ($V_{\mathrm{dc-I}} = -0.1$ mV and $V_{\mathrm{dc-Q}} = -0.2$ V) for a maximum carrier suppression of -60 dB relative to the sidebands. Then, the LSB was minimized to -70 dB relative to the upper by adjusting the imbalance parameters ($\psi = -0.84^{\circ}$ and $\varepsilon = 0.04$ dB). The modulator DDSs were configured for PM generation (see Table II). The spurious AM was monitored at the output of the AM detector and nulled by adjusting the phase shift to $\theta = 130^{\circ}$. At this point, the modulator impairments are determined and used to produce relatively pure AM and PM. Next, the carrier and sideband powers were measured by following the calibration procedure described in Section IV. Using these measured

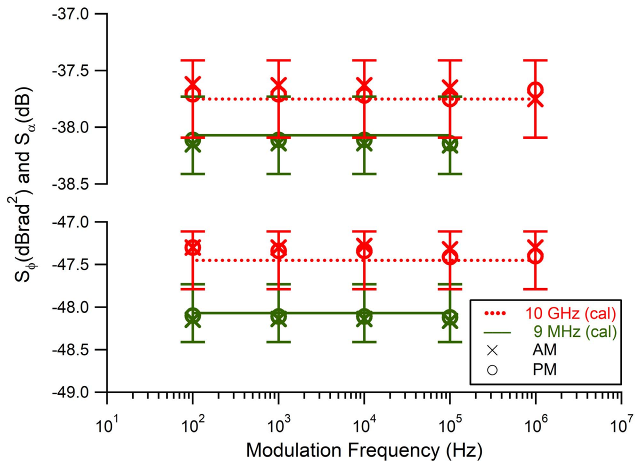

Fig. 8. Variation of the AM and PM with modulation frequency for 9-MHz and 10-GHz modulators.

power levels in conjunction with the measurement equations (12), (13), and (17), the level of the PM was calculated to be $S_{\varphi}(f_m) = -38.1 \pm 0.3$ dBrad^2, and the level AM was $S_{\alpha}(f_m) = -38.1 \pm 0.3$ dB. The uncertainty (coverage factor $k = 2$) was determined from the values given in Table IV. The "Type A" uncertainties were calculated by performing statistics on a series of repeated measurements, and the "Type B" uncertainties were determined by creating uniform probability distributions from a range of observed values, manufacturer specifications, or calibration reports. The observed values were collected by measuring the minimum and maximum variation of a parameter as the modulator varied through its full range of θ and f_m.

The modulated signals from the primary output of the modulator were then demodulated and measured on the FFT analyzer and compared to the calculated PM and AM levels. The PM and AM tones were measured to be $S_{\varphi}(100\text{ kHz}) = -38.1$ dBrad^2, and $S_{\alpha}(100\text{ kHz}) = -38.2$ dB, with spurious modulations of $S_{\alpha}(100\text{ kHz}) = -93$ dB and $S_{\varphi}(100\text{ kHz}) = -89$ dBrad^2, respectively. The modulation frequency was varied from 100 Hz to 100 kHz, and we observed a flat frequency response of <0.03 dB without recalibrating the modulator. We were able to measure the FOM of approximately 0.3 ppm on the diode detector for the PM modulator. However, when measured on the FFT digital demodulator, the FOM for both AM and PM varied between 1 and 8 ppm for different f_m values. This loss of FOM is most likely due to the nonlinearity of the analog-to-digital converters in the FFT analyzer.

The same procedure described above was repeated for different modulation depths and modulation frequencies for both 9-MHz and 10-GHz carriers. The calibrated and measured AM and PM are shown in Fig. 8. A summary of the experimental evaluation of the modulators at 9 MHz and 10 GHz is also provided in Table V. It shows the error between the measured and calculated modulation levels for both AM and PM versus frequency and two modulation depths. The error includes the uncertainty ($k = 2$) of the calculated level and the uncertainty of AM/PM noise standard [16] used to verify the accuracy of the FFT demodulator. The FOM was measured on both the diode detector and the FFT analyzer.

TABLE IV

FRACTIONAL ERRORS USED FOR UNCERTAINTY CALCULATION AT 9 MHZ

Sources of Error and Symbol	Logarithmic		Type	Distribution	Divisor	Sensitivity Multiplier	Standard Fractional Uncertainty (σ), %
	Value, dB(m)	Error dB					
Measurement of sideband power, σ_{DSB}	–45.9	0.1	A	Normal	1	1.0	2.3%
Measurement of carrier power, $\sigma_{P_C'}$	–36.4	0.1	A	Normal	1	1.0	2.3%
SNR for sideband power measurement, σ_{SNR}	30.0	5.0	B	Uniform	1.73	1.0E–03	0.1%
SNR for carrier power measurement, $\sigma_{SNR'}$	40.0	5.0	B	Uniform	1.73	1.0E–04	0.0%
Attenuator, σ_A	28.6	0.2	B	Uniform	1.73	1.0	2.0%
Switch repeatability, σ_{SW}	0.0	0.0	B	Uniform	1.73	1.0	0.1%
Power meter nonlinearity, σ_{PNL}	0.0	0.1	B	Uniform	1.73	1.0	0.7%
Harmonic content, $\sigma_{\delta h}$	–58.0	5.0	B	Uniform	1.73	1.6E–06	0.0%
Unsuppressed Carrier, $\sigma_{\delta c}$	–62.0	3.0	B	Uniform	1.73	3.2E–07	0.0%
Spurious AM, σ_κ	–64.0	8.0	B	Uniform	1.73	4.0E–07	0.0%
SSB imbalance (δ_{ssb}= –60 dB), $\sigma_{\kappa ssb}$	0.0	0.0	B	Uniform	1.73	1.0	0.2%

TABLE V

SUMMARY OF THE EXPERIMENTAL EVALUATION OF THE MODULATORS AT 9 MHZ AND 10 GHZ

Mod Depth	f_m kHz	9 MHz					10 GHz				
		PM			AM		PM			AM	
		Error dB	FOM Diode ppm	FOM FFT ppm	Error dB	FOM FFT ppm	Error dB	FOM Diode ppm	FOM FFT ppm	Error dB	FOM FFT ppm
≈0.006	1000	-	-	-	-	-	-0.1 ± 0.4	40	1000	-0.2 ± 0.4	631
	100	0.1 ± 0.4	0.2	3	0.1 ± 0.4	8	0 ± 0.4	1	200	-0.1 ± 0.4	63
	10	0 ± 0.4	0.3	5	0.1 ± 0.4	4	-0.1 ± 0.4	79	200	-0.2 ± 0.4	63
	1	0 ± 0.4	0.3	2	0.1 ± 0.4	4	-0.1 ± 0.4	100	20	-0.2 ± 0.4	126
	0.1	0 ± 0.4	0.3	<1	0.1 ± 0.4	3	-0.2 ± 0.4	10	501	-0.2 ± 0.4	1000
≈0.018	1000	-	-	-	-	-	-0.1 ± 0.4	25	126	0 ± 0.4	398
	100	0 ± 0.4	0.6	<4	0.1 ± 0.4	<4	0 ± 0.4	1	200	-0.1 ± 0.4	10
	10	0 ± 0.4	0.6	<4	0.1 ± 0.4	<4	0 ± 0.4	100	200	-0.1 ± 0.4	20
	1	0 ± 0.4	1	3	0.1 ± 0.4	3	0 ± 0.4	20	100	-0.1 ± 0.4	316
	0.1	0 ± 0.4	1	3	0.1 ± 0.4	5	0 ± 0.4	4	158	-0.1 ± 0.4	316

'<' indicates noise floor limitation.

The 9-MHz modulator was able to create and maintain PM with spurious AM (κ as measured on the diode detector) at a level of <1 ppm even as the modulation frequency was varied. The modulation depth was decreased by approximately 10 dB, and after reoptimizing, the modulator also performed at the <1 ppm level. Using the digital demodulation on the FFT, FOM (κ and γ) measurements ranged between 1 and 8 ppm for both PM and AM as modulation frequency and depth varied.

For the 10-GHz modulator, κ measured on the diode ranged between 1 and 100 ppm. Even when levels of 1 ppm were achieved, they would eventually drift toward 100 ppm as environmental effects disturbed the alignment of the modulator. When measuring FOM using the downconverter and FFT, spurious levels between 10 and 1000 ppm were observed. This increase in the FOM was due to the nonlinearity of the downconverter stage.

We compared the performance of the 9-MHz IQ modulator with the traditional Armstrong modulator constructed with a single mixer and an RF phase shifter. To replicate a single mixer configuration, we inserted a manual phase shifter between the input coupler and the LO input of the IQ mixer (see Fig. 4) and only used the I input while terminating the Q input with 50 Ω. This way, we ensured that the same nonlinear components were used in the comparison. Both the traditional and IQ modulators were able to generate PM signals with FOM of <1 ppm; however, we found that it was easier to suppress the spurious AM in the IQ modulator because the phase shift could be generated digitally with finer resolution and without backlash. Furthermore, the advantage of being able to toggle between AM, PM, and SSB with a software adjustable phase shift justifies the extra complexity of the IQ modulator configuration for use in AM/PM noise metrology.

VI. CONCLUSION

In this work, we discussed the working principle of an IQ-based Armstrong modulator as a calibrator for precision PM and AM noise measurements. We highlighted the impairments associated with such a modulator and proposed a simple method that uses SSB modulation for the correction of these impairments. This modulator can be used in line with any PM and AM noise measurement system without needing a calibrated IQ demodulator for high-purity PM and AM alignment and generation. We also described the calibration procedure and provided a detailed uncertainty analysis for this modulator.

We built two modulators at 9 MHz and 10 GHz with PM and AM uncertainty equal to ± 0.3 dB. We achieved an FOM of less than 1 ppm and less than 100 ppm for the 9-MHz and 10-GHz modulators, respectively. Additionally, we also showed that the FFT digital demodulator is capable of measuring FOM less than 10 ppm.

ACKNOWLEDGMENT

The authors would like to thank Jeff Sherman, Vladislav Gerginov, Daniel Slichter, and Connor Humiston for their scientific and editorial comments on this manuscript. They would also like to thank Corey Barnes for his contribution to the initial dual DDS programming.

This work is a contribution of the National Institute of Standards and Technology (NIST), Boulder, CO, USA, an agency of the U.S. Government, and is not subject to copyright. Commercial products are indicated in this document for completeness; no endorsement is implied.

REFERENCES

[1] A. L. Lance, W. D. Seal, and F. Labbar, "Phase noise and AM measurements in the frequency domain," in *Infrared and Millimeter Waves*, vol. 11, 1984, pp. 284–286.

[2] F. L. Walls and E. Ferre-Pikal, "Measurement of frequency, phase noise and amplitude noise," in *Wiley Encyclopedia of Electrical and Electronics Engineering*, vol. 12, 1st ed. Hoboken, NJ, USA: Wiley, 1999, pp. 459–473.

[3] E. Rubiola and V. Giordano, "Correlation-based phase noise measurements," *Rev. Sci. Instrum.*, vol. 71, no. 8, pp. 3085–3091, Aug. 2000, doi: 10.1063/1.1304871.

[4] C. W. Nelson, A. Hati, and D. A. Howe, "A collapse of the cross-spectral function in phase noise metrology," *Rev. Sci. Instrum.*, vol. 85, no. 3, Feb. 2014, Art. no. 024705, doi: 10.1063/1.4865715.

[5] A. Hati, C. W. Nelson, and D. A. Howe, "Cross-spectrum measurement of thermal-noise limited oscillators," *Rev. Sci. Instrum.*, vol. 87, no. 3, Mar. 2016, Art. no. 034708, doi: 10.1063/1.4944808.

[6] E. H. Armstrong, "A method of reducing disturbances in radio signaling by a system of frequency modulation," *Proc. Inst. Radio Eng.*, vol. 24, no. 5, pp. 689–740, May 1936, doi: 10.1109/JRPROC.1936.227383.

[7] K. H. Sann, "The measurement of near-carrier noise in microwave amplifiers," *IEEE Trans. Microw. Theory Techn.*, vol. MTT-16, no. 9, pp. 761–766, Sep. 1968, doi: 10.1109/TMTT.1968.1126783.

[8] F. L. Walls, "Frequency calibration standard using a wide band phase modulator," U.S. Patent 5 101 506 A, Mar. 31, 1992. [Online]. Available: https://patents.google.com/patent/US5101506/en

[9] F. L. Wall, "Correlation between upper and lower sidebands," *IEEE Trans. Ultrason., Ferroelectr., Freq. Control*, vol. 47, no. 2, pp. 407–410, Mar. 2000, doi: 10.1109/58.827427.

[10] F. L. Walls, "Secondary standard for PM and AM noise at 5, 10, and 100 MHz," *IEEE Trans. Instrum. Meas.*, vol. 42, no. 2, pp. 136–143, Apr. 1993, doi: 10.1109/19.278536.

[11] F. L. Walls, A. J. D. Clements, C. M. Felton, M. A. Lombardi, and M. D. Vanek, "Extending the range and accuracy of phase noise measurements," in *Proc. 42nd Annu. Freq. Control Symp.*, Jun. 1988, pp. 432–441, doi: 10.1109/FREQ.1988.27636.

[12] E. Rubiola, "Primary calibration of AM and PM noise measurements," 2009, *arXiv:0901.1073*.

[13] E. N. Ivanov, "Generation of pure phase and amplitude-modulated signals at microwave frequencies," *Rev. Sci. Instrum.*, vol. 83, no. 6, Jun. 2012, Art. no. 064705, doi: 10.1063/1.4729477.

[14] *IEEE Draft Standard Definitions of Physical Quantities for Fundamental Frequency and Time Metrology-Random Instabilities*, Standard IEEE P1139/D16, Nov. 2021, pp. 1–45.

[15] B. P. Lathi, *Modern Digital and Analog Communications Systems*. New York, NY, USA: Henry Holt & Company, 1983.

[16] A. Hati, C. W. Nelson, N. Ashby, and D. A. Howe, *Calibration Uncertainty for the NIST PM/AM Noise Standards*, document NIST Special Publication 250–90, Jul. 2012.

[17] *Evaluation of Measurement Data Guide to the Expression of Uncertainty in Measurement*, BIPM, Sèvres, France, 2008.

[18] R. L. Filler, "The acceleration sensitivity of quartz crystal oscillators: A review," *IEEE Trans. Ultrason., Ferroelectr., Freq. Control*, vol. UFFC-35, no. 3, pp. 297–305, May 1988, doi: 10.1109/58.20450.

[19] B. N. Taylor and C. E. Kuyatt, "Guidelines for evaluating and expressing the uncertainty of NIST measurement results," NIST, Gaithersburg, MD, USA, Tech. Note 1297, 1994.

[20] E. Rubiola, "The measurement of AM noise of oscillators," Dec. 2005, *arXiv:physics/0512082*.

Archita Hati (Member, IEEE) received the M.Sc. degree in physics, the M.Phil. degree in microwaves, and the Ph.D. degree in physics from the University of Burdwan, Bardhaman, India, in 1992, 1993, and 2001, respectively.

She is currently an Electronics Engineer with the Time and Frequency Division, National Institute of Standards and Technology, Boulder, CO, USA, where she is the Calibration Service Leader of the Time and Frequency Metrology Group. Her current research interests include phase noise metrology, ultralow noise frequency synthesis, development of low-noise microwave and optoelectronic oscillators, and vibration analysis.

Dr. Hati has been an Associate Editor of the IEEE TRANSACTIONS ON ULTRASONICS, FERROELECTRICS, AND FREQUENCY CONTROL since 2021. She was a recipient of the Allen V. Astin Measurement Science Award "for developing a world-leading program of phase noise research and measurement services to support industry and national priorities" in 2015.

Craig W. Nelson (Member, IEEE) received the B.S.E.E. degree in electrical engineering from the University of Colorado at Boulder, Boulder, CO, USA, in 1990.

He is currently an Electrical Engineer with the Time and Frequency Division, National Institute of Standards and Technology (NIST), Boulder. He has authored over 70 papers and teaches classes, tutorials, and workshops at NIST, the IEEE Frequency Control Symposium, and several sponsoring agencies on the practical aspects of high-resolution phase noise metrology.

Mr. Nelson was a recipient of the NIST Bronze Medal in 2012, the Allen V. Astin Measurement Science Award "for developing a world-leading program of phase noise research and measurement services to support industry and national priorities" in 2015, and the IEEE Cady Award "for leadership in the design and development of state-of-the-art low noise oscillators and phase noise measurement systems" in 2020.